Supporting Information

A new Schiff-based chemosensor for chromogenic sensing of Cu^{2+}, Co^{2+} and S^{2-} in aqueous solution: experimental and theoretical studies

Cheol Hong Min,[a] Sangkyun Na,[a] Jae Eun Shin,[a] Jae Kyun Kim,[a] Tae Geun Jo,[b]* Cheal Kim*[a,b]

[a] *Nowon Institute of Education for The Gifted at Seoultech, Seoul National University of Science and Technology, Seoul 139-743, Korea*

Department of Fine Chemistry and Department of Interdisciplinary Bio IT Materials, Seoul National University of Science and Technology, Seoul 139-743, Republic of Korea. Fax: +82-2-973-9149; Tel: +82-2-970-6693; E-mail: jtgjjj@nate.com and chealkim@seoultech.ac.kr

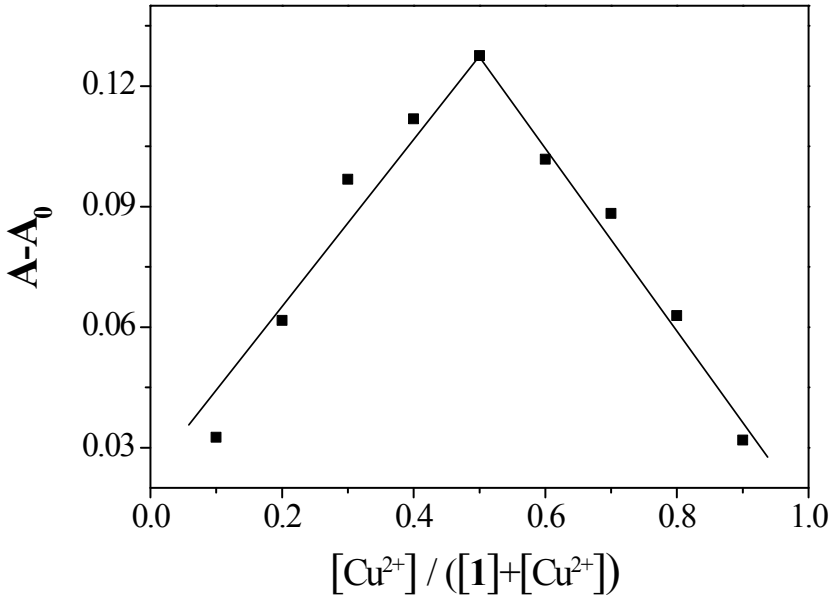

Fig. S1 Job plot of **1** (40 μM) with Cu^{2+}, where the absorbance at 409 nm was plotted against the mole fraction of Cu^{2+}.

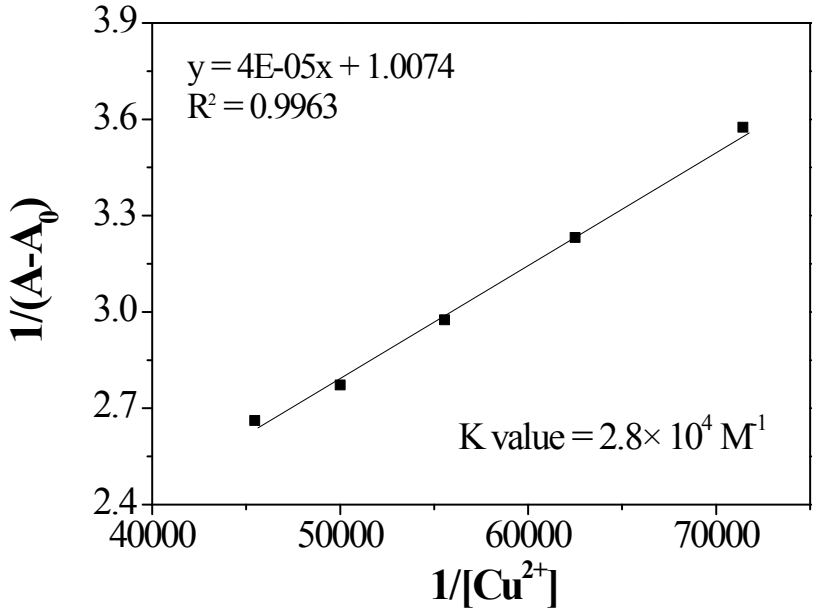

Fig. S2 Benesi-Hildebrand plot of **1** (20 μM) for Cu^{2+}, assuming 1:1 stoichiometry for association of **1** with Cu^{2+}.

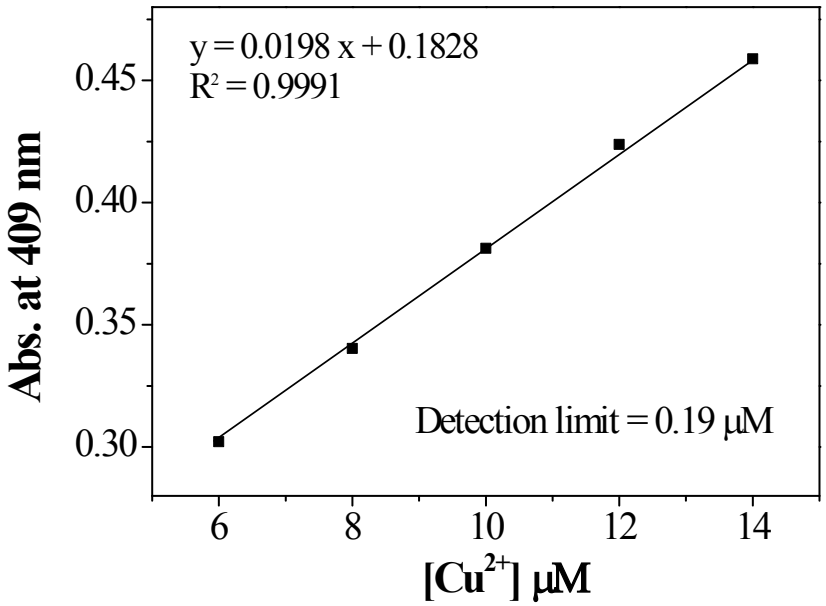

Fig. S3 Determination of the detection limit of **1** (20 μM) for Cu^{2+} based on change of absorbance at 409 nm.

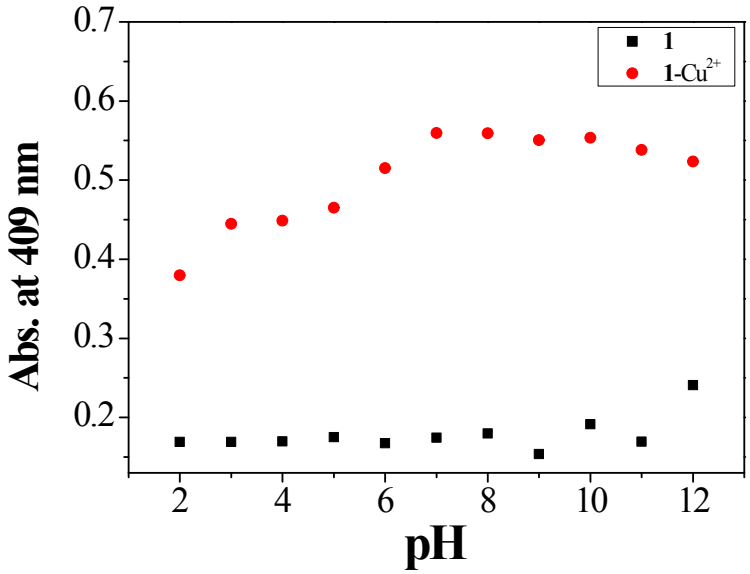

Fig. S4 UV-vis absorbance changes (at 409 nm) of **1** (20 μM) and **1**-Cu^{2+} complex, respectively, in different pH (2-12) solutions (bis-tirs buffer/THF (1/1, v/v)).

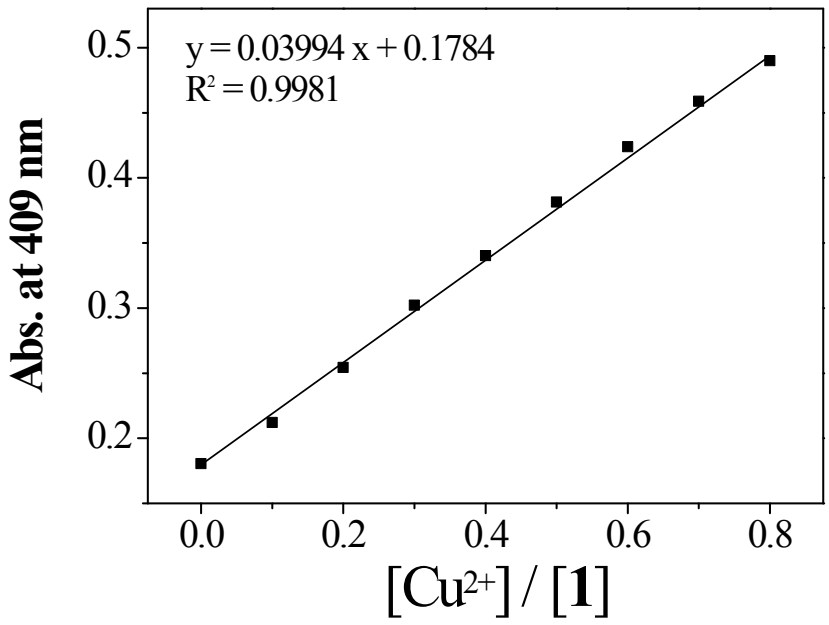

Fig. S5 UV-vis absorbance (at 409 nm) of **1** as a function of Cu^{2+} concentration. [**1**] = 20 μM and [Cu^{2+}] = 0-16 μM.

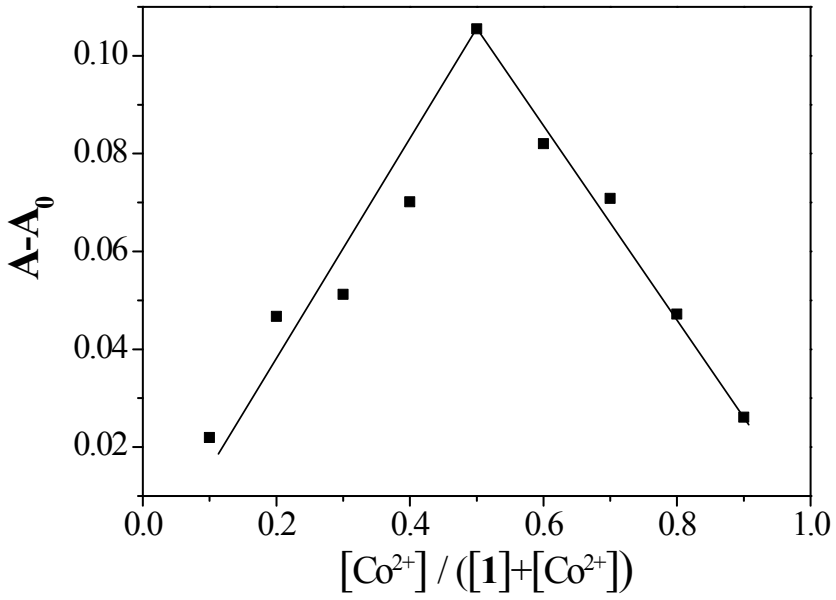

Fig. S6 Job plot of **1** (40 μM) with Co^{2+}, where the absorbance at 427 nm was plotted against the mole fraction of Co^{2+}.

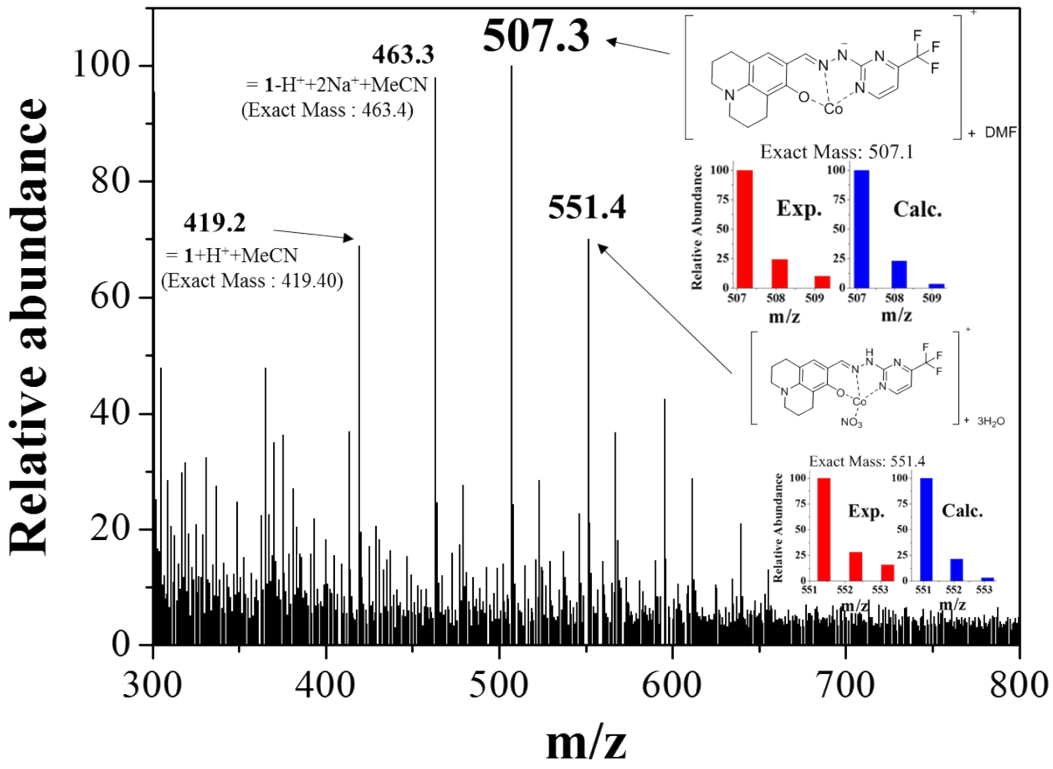

Fig. S7 Positive-ion ESI-mass spectrum of **1** (100 μM) upon addition of 1 equiv of Co^{2+}.

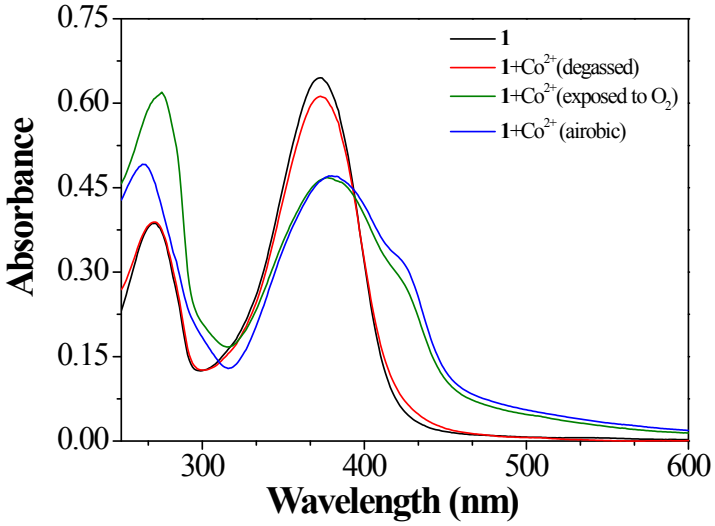

Fig. S8 Absorption spectra of **1** (20 μM), **1**-Co^{2+} complex under the degassed and exposure-to-air conditions, and **1**-Co^{2+} complex under aerobic conditions, respectively.

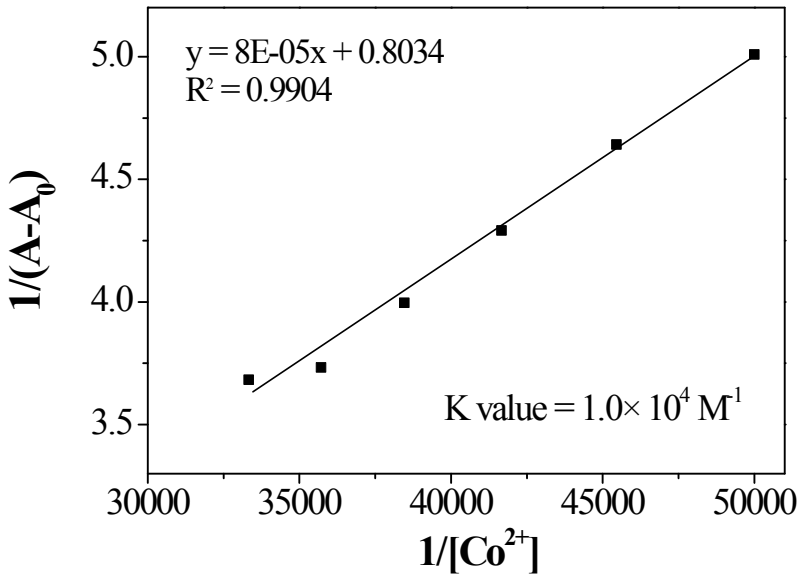

Fig. S9 Benesi-Hildebrand plot of **1** (20 μM) for Co^{2+}, assuming 1:1 stoichiometry for association of **1** with Co^{2+}.

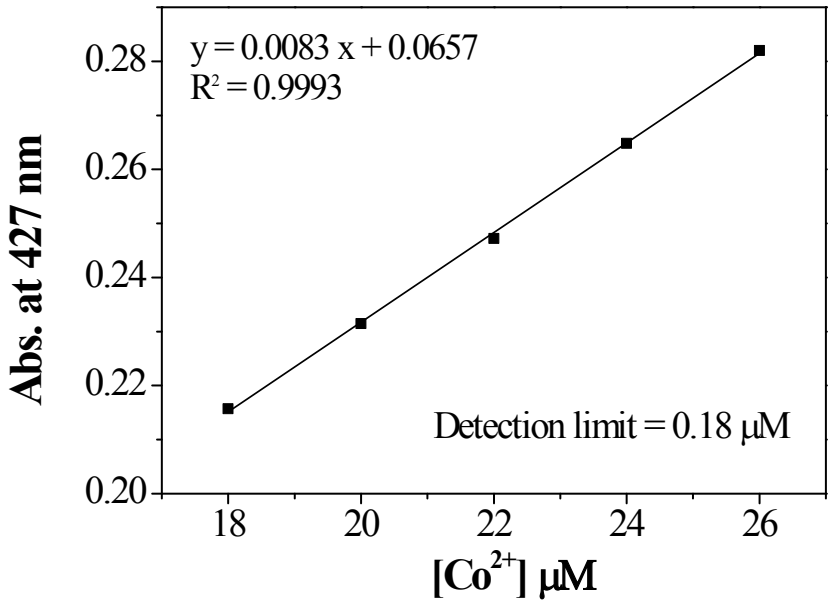

Fig. S10 Determination of the detection limit of **1** (20 μM) for Co^{2+} based on change of absorbance at 427 nm.

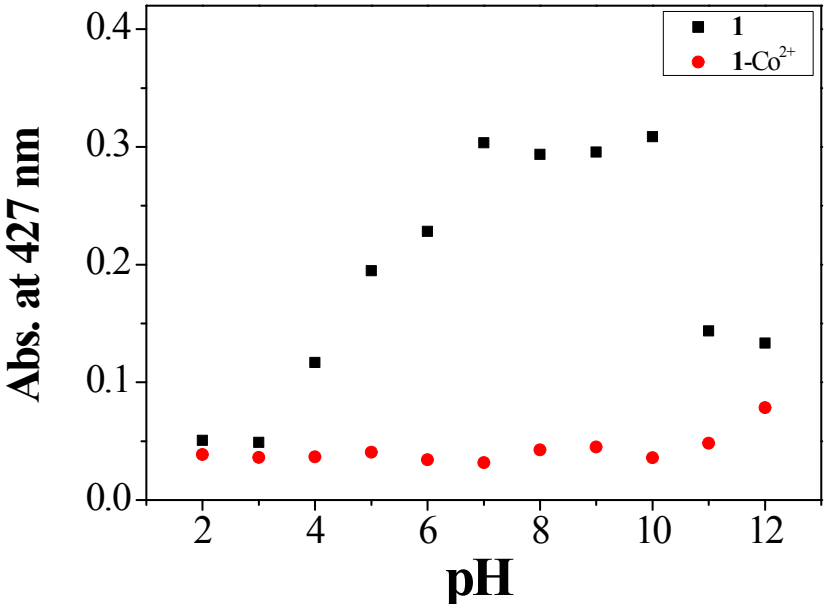

Fig. S11 UV-vis absorbance changes (at 427 nm) of **1** (20 μM) and **1**-Co^{2+} complex, respectively, in different pH (2-12) solution (bis-tirs buffer/THF (1/1, v/v)).

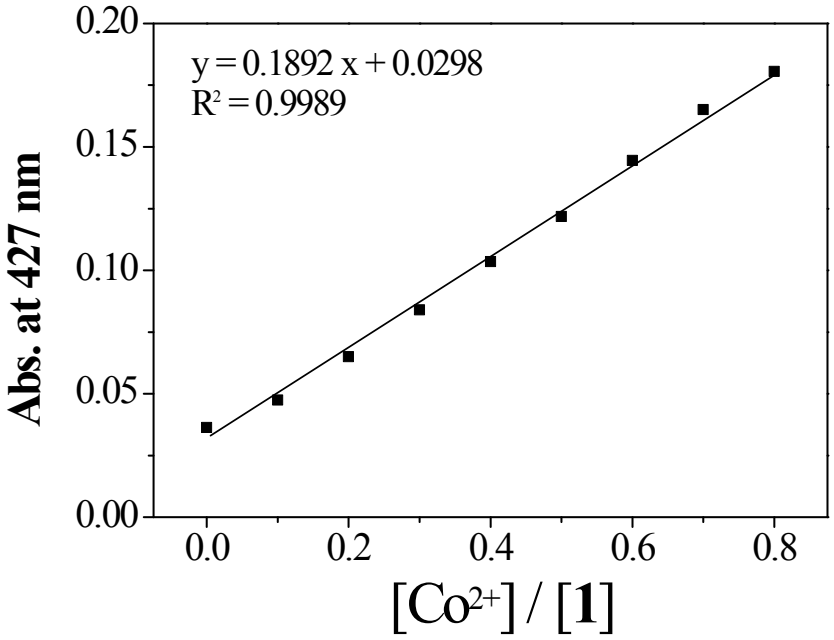

Fig. S12 UV-vis absorbance (at 427 nm) of **1** as a function of Co^{2+} concentration. [**1**] = 20 μM and [Co^{2+}] = 0-16 μM.

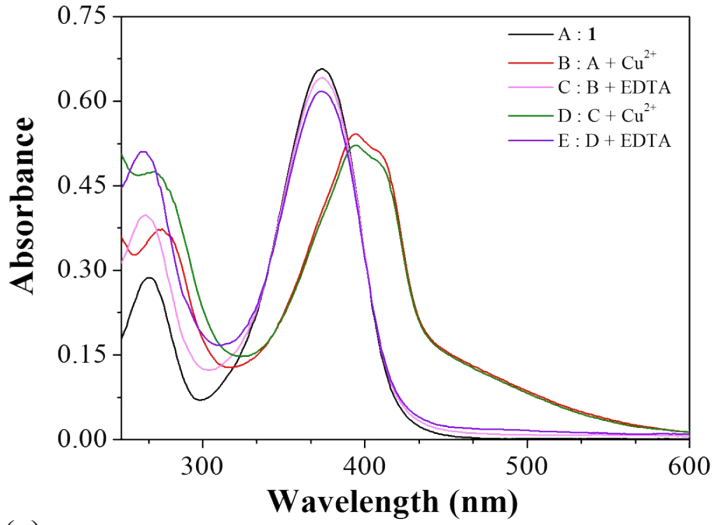

(a)

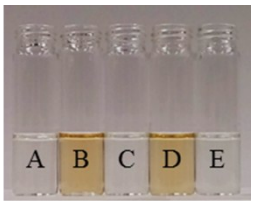

(b)

Fig. S13 (a) UV-vis spectral and (b) color changes of **1** (20 μM) after the sequential addition of Cu^{2+} (1.2 equiv) and EDTA (1.8 equiv).

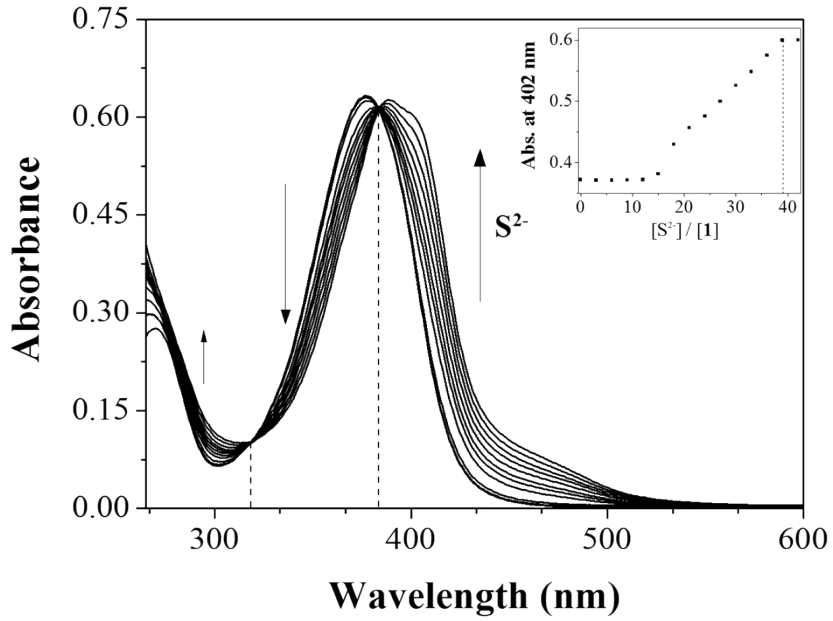

Fig. S14 UV-vis spectral change of **1** (20 μM) with S^{2-} (0-42 equiv) in bis-tris buffer/DMSO (1/9, v/v).

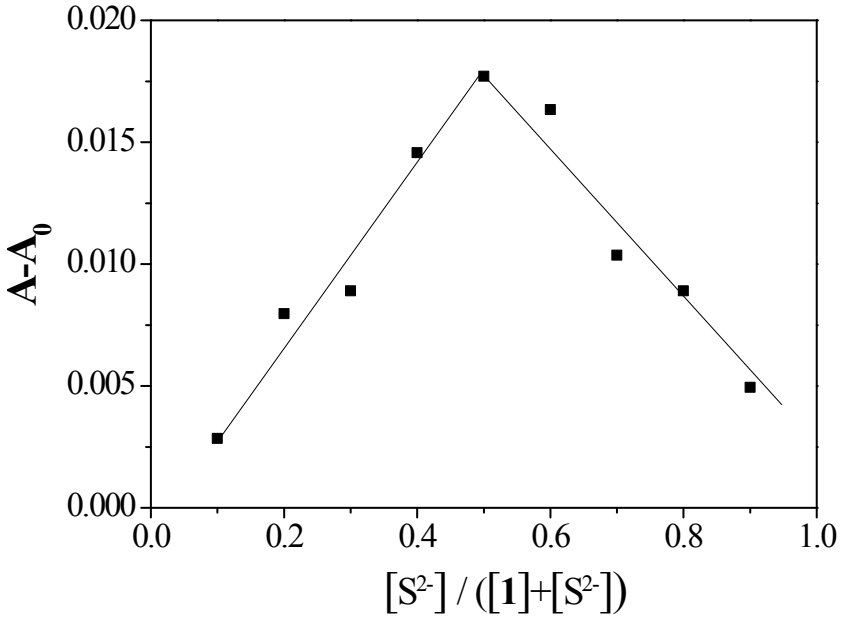

Fig. S15 Job plot of **1** (100 μM) with S^{2-}, where the absorbance at 402 nm was plotted against the mole fraction of S^{2-}.

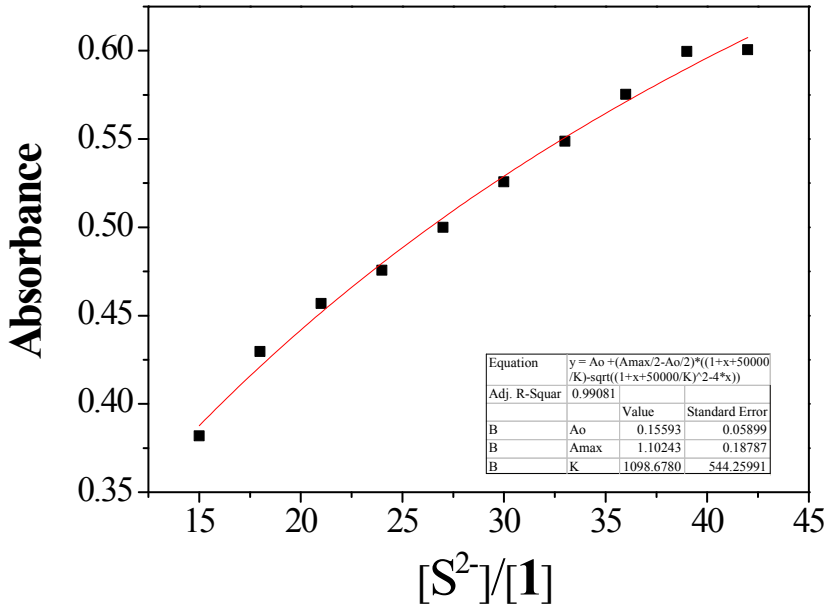

Fig. S16 UV-vis absorbance of **1** (20 μM) after addition of increasing different concentration of S^{2-}. The red line is the non-linear fitting curve between **1** and S^{2-}. Association constant (*K*) of **1** with S^{2-} was calculated by non-linear least square curve fitting.

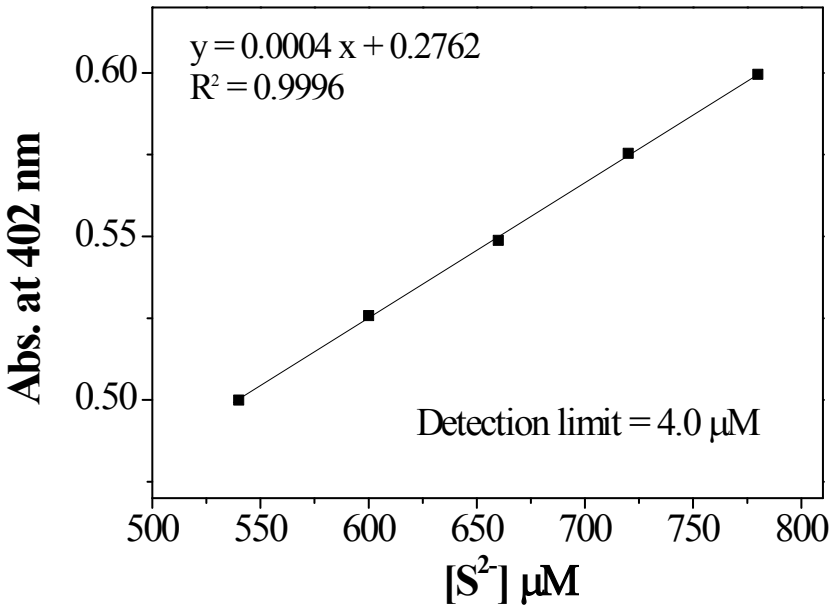

Fig. S17 Determination of the detection limit of **1** (20 μM) for S^{2-} based on change of absorbance at 402 nm.

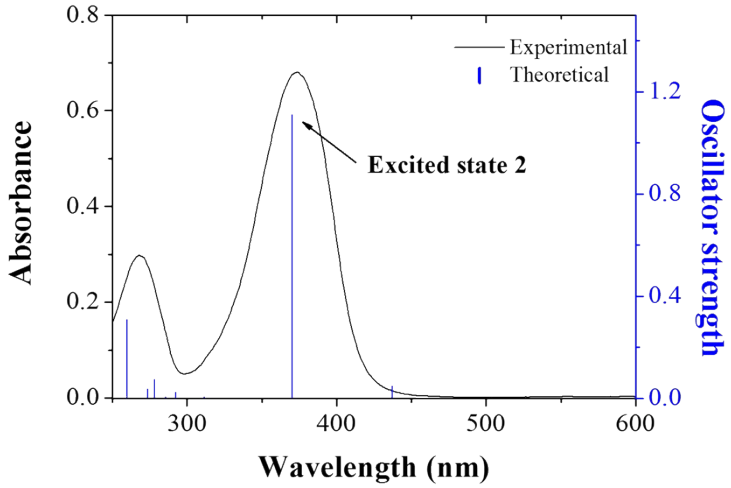

(a)

Excited State 2	Wavelength	Percent (%)	Character	Oscillator strength
H → L+1	370.18	97%	ICT	1.111

(b)

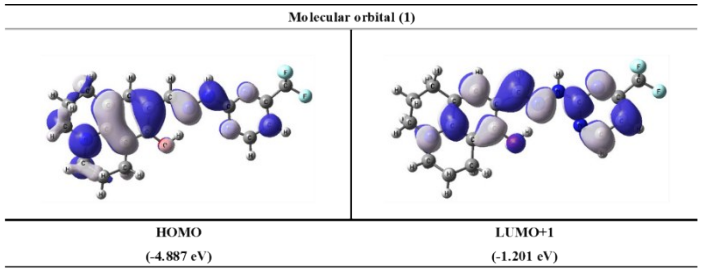

(c)

Fig. S18 (a) Blue bars are the theoretical excitation energies (TD-DFT method) and black curve is the experimental UV-vis spectrum of **1**. (b) The major electronic transition energy and molecular orbital contribution for **1** (H = HOMO and L = LUMO). (c) Isosurface (0.030 electron bohr 3) of molecular orbitals participating in the major singlet excited state of **1**.

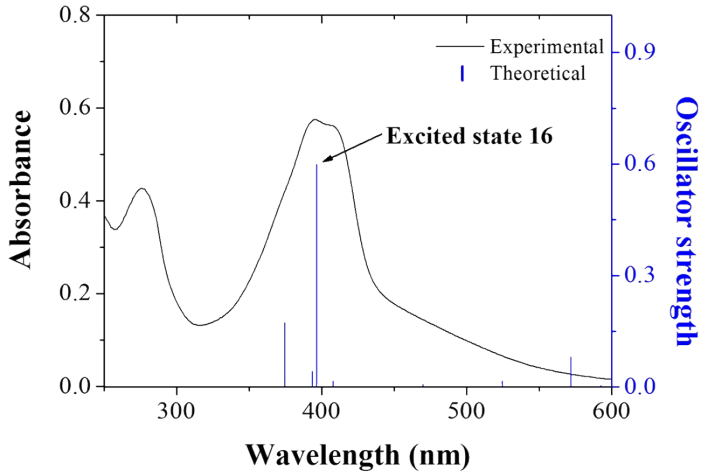

(a)

Excited State 16	Wavelength	percent (%)	Character	Oscillator strength
H (α) → L+2 (α)	396.84	36%	ICT	0.598
H (β) → L+3 (β)		37%	ICT	
H-4 (β) → L (β)		4%	LMCT	
H-1 (β) → L+2 (β)		4%	LMCT	
H-25 (β) → L (β)		3%	LMCT	
H-1 (α) → L+2 (α)		2%	ICT	
H-1 (β) → L+3 (β)		2%	ICT	
H-2 (β) → L (β)		2%	LMCT	

(b)

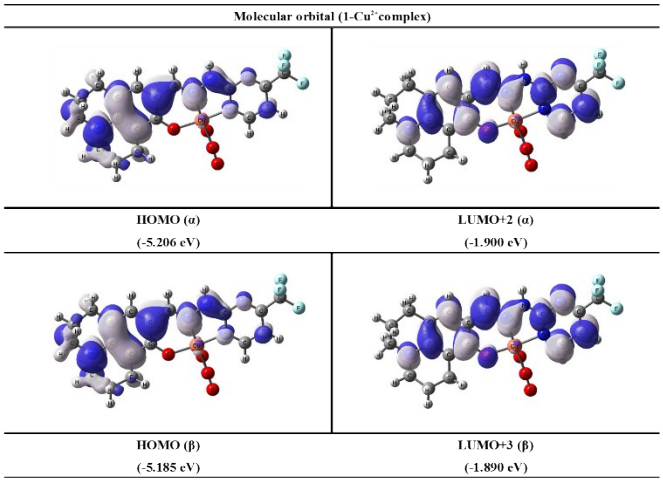

(c)

Fig. S19 (a) Blue bars are the theoretical excitation energies (TD-DFT method) and black curve is the experimental UV-vis spectrum of **1**-Cu^{2+}. (b) The major electronic transition energies and molecular orbital contributions for **1**-Cu^{2+} (H = HOMO and L = LUMO). (c) Isosurface (0.030 electron bohr 3) of molecular orbitals participating in the major singlet excited state of **1**-Cu^{2+}.

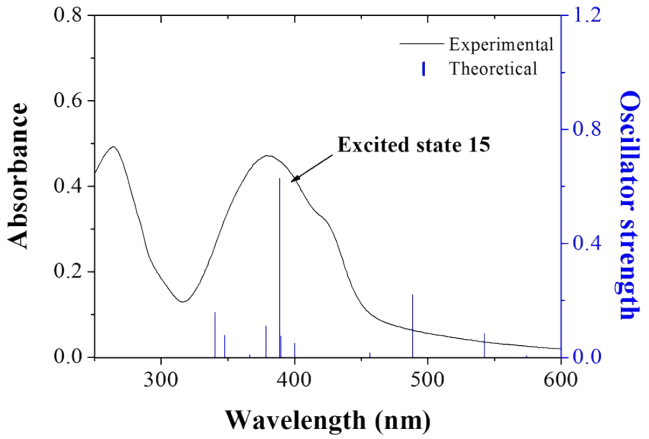

(a)

Excited State 16	Wavelength	Percent (%)	Character	Oscillator strength
H → L+5	390.81	64%	LMCT	0.6878
H-1 → L+4		16%	ICT, LMCT	
H-3 → L		3%	ICT, LMCT	
H → L+4		3%	ICT, LMCT	

(b)

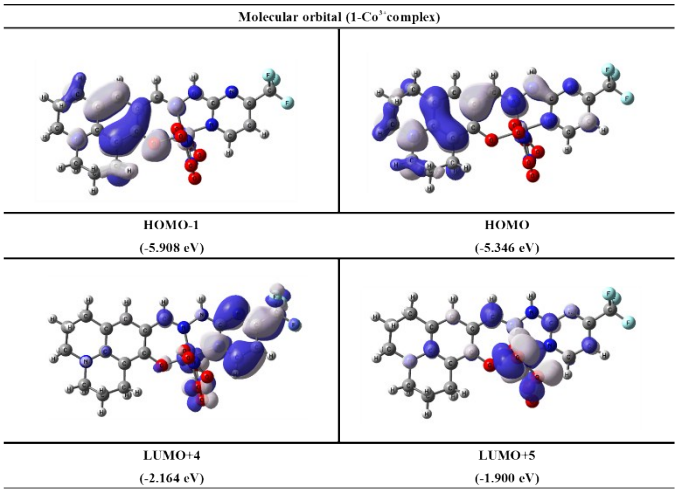

(c)

Fig. S20 (a) Blue bars are the theoretical excitation energies (TD-DFT method) and black curve is the experimental UV-vis spectrum of **1**-Co^{3+}. (b) The major electronic transition energies and molecular orbital contributions for **1**-Co^{3+} (H = HOMO and L = LUMO). (c) Isosurface (0.030 electron bohr 3) of molecular orbitals participating in the major singlet excited state of **1**-Co^{3+}.

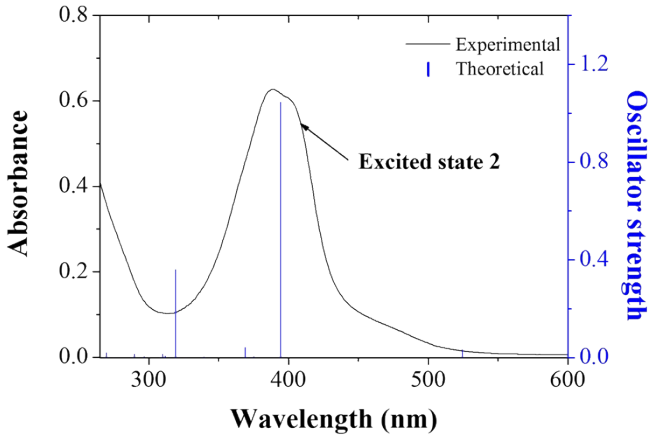

(a)

Excited State 2	Wavelength	Percent (%)	Character	Oscillator strength
H → L+1	394.47	97%	ICT	1.046

(b)

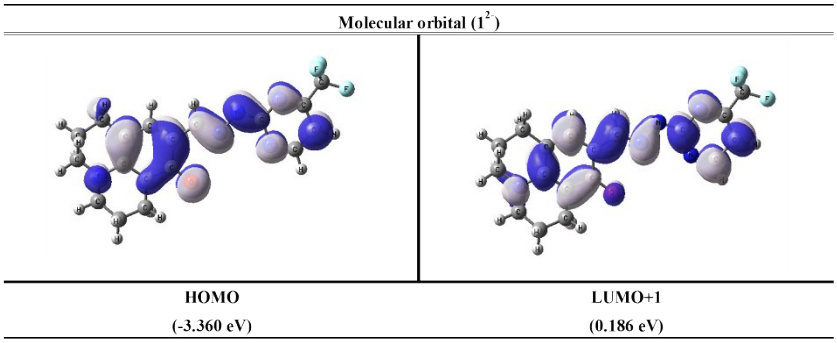

(c)

Fig. S21 (a) Blue bars are the theoretical excitation energies (TD-DFT method) and black curve is the experimental UV-vis spectrum of $\mathbf{1}^{2-}$. (b) The major electronic transition energy and molecular orbital contribution for $\mathbf{1}^{2-}$ (H = HOMO and L = LUMO). (c)

Isosurface (0.030 electron bohr 3) of molecular orbitals participating in the major singlet excited state of $\mathbf{1}^{2-}$.